AAPS PharmSciTech (2023) 24:56
https://doi.org/10.1208/s12249-023-02517-8

RESEARCH ARTICLE

Synthesis of Submicrometric Chitosan Particles Loaded with Calcium Phosphate for Biomedical Applications

Diana Pereira Lopes[1] · Selma Regina Muniz Freitas[2] · Carina Baptiston Tanaka[3] · Giovanne Delechiave[4] · Lucia Nobuco Takamori Kikuchi[1] · Roberto R. Braga[5] · Jamie J. Kruzic[6] · Maria Stella Moreira[1] · Leticia Cristina Cidreira Boaro[2] · Luiz Henrique Catalani[4] · Flávia Gonçalves[2]

Received: 16 June 2022 / Accepted: 16 January 2023

Abstract

Chitosan particles loaded with dibasic calcium phosphate *anhydrous* (DCPA) is a promising strategy for combining antimicrobial and osteoconduction properties in regenerative medicine. However, mostly micrometer-sized particles have been reported in the literature, limiting their use and reducing their effect in the biomedical field. We have recently overcome this limitation by developing submicrometer-sized particles with electrospray technique. The objective of this study was to understand how the process parameters control the size and properties of submicrometer chitosan particles loaded with DCPA. Solutions of 10 mg/mL chitosan and 2.5 mg/mL DCPA in a 90% acetic acid were electrosprayed under three distinct flow rate conditions: 0.2, 0.5, and 1.0 mL/h. The particles were crosslinked in a glutaraldehyde atmosphere and characterized in terms of their morphology, inorganic content, zeta potential, and minimum inhibitory concentration (MIC) against *S. mutans*. All conditions showed particles with two similar morphologies: one small-sized with a spherical shape and another larger-sized with a bi-concave shape. All generated a broad particle size distribution, with a similar mean size of ~ 235 nm. The addition of DCPA decreased the zeta potential for all the samples, but it was above 30 mV, indicating a low aggregation potential. The lower flow rate showed the worst efficacy for DCPA incorporation. Antimicrobial activity was greater in chitosan/DCPA particles with flow rate of 0.5 mL/h. It can be concluded that the flow rate of 0.5 mL/h presents the best compromise solution in terms of morphology, zeta potential, MIC, and inorganic content.

Keywords chitosan particles · dibasic calcium phosphate · electrospray · minimum inhibitory concentration · *S. mutans* · zeta potential

✉ Leticia Cristina Cidreira Boaro
leticiacidreiraboaro@gmail.com; lboaro@prof.unisa.br

[1] Departamento de Odontologia, Universidade Ibirapuera, Av. Interlagos 1329 – 4° andar, São Paulo, SP 04661-100, Brazil

[2] Faculdade de Odontologia, Universidade Santo Amaro, Av. Prof. Eneas de Siqueira Neto, 340, São Paulo, SP 04829-900, Brazil

[3] Centre for Rural Dentistry & Oral Health, Charles Sturt University, Orange, NSW 2800, Australia

[4] Departamento de Química Fundamental, Instituto de Química da Universidade de São Paulo, Av. Prof. Lineu Prestes, 748, São Paulo, SP 05508-000, Brazil

[5] Faculdade de Odontologia da Universidade de São Paulo, Departamento de Biomateriais e Biologia Oral, Av. Prof. Lineu Prestes, 2222, São Paulo, SP 05508-000, Brazil

[6] School of Mechanical and Manufacturing Engineering, University of New South Wales (UNSW Sydney), Sydney, NSW 2052, Australia

Introduction

Bacterial contamination plays a major role in the failure of resin-based dental restorations due to secondary caries, as well as in causing complications after root canal treatment and surgical procedures [1–3]. Therefore, the development of functional materials capable of stimulating tissue formation and/or reducing bacterial growth has become the focus of several research groups [4–12].

Numerous antimicrobial compounds have been suggested to inhibit biofilm formation, such as chlorhexidine [5], triclosan [6], bioactive glass fillers [7, 8], and novel monomers [9–12]. Because there is an increased need to develop sustainable bio-based materials with antimicrobial properties, chitosan is a promising material for dental applications [13–15]. Chitosan is a natural polymer with low toxicity and osteoconductive and antimicrobial properties [16]. It has a wide range of applications

Published online: 09 February 2023

in the dental and medical fields as a drug delivery agent and in the food and textile industry as an antimicrobial preservative. Besides its antimicrobial benefits, chitosan production has emerged as a potential economic and environmentally sustainable solution for the reprocessing of biowaste [17].

Additionally, calcium phosphate-based materials are well known in dental and orthopedic fields for their ion release and remineralization properties [18–20]. Incorporating chitosan and calcium phosphate into a single particle has the potential to generate versatile bioactive particles that can be incorporated in different matrices for several applications, such as bone regeneration, dental caries prevention, and control of periodontal and endodontic infections. The synthesis of chitosan/dibasic dicalcium phosphate or chitosan/calcium carbonate particles by double emulsion techniques has been reported, with an average diameter of 30–60 µm [21, 22], as well as core-shell particles with an average size of 350 µm [23]. However, for these hybrid particles to be used in polymeric dental materials, much smaller sizes (2 µm or less) are necessary to avoid impairing their mechanical properties [24].

To overcome this limitation, it has been recently developed an electrospray technique to produce particles with nano- to submicrometric sizes [25]. The method consists of pumping a positively charged polymeric solution through a needle and establishing an electric field between the needle and collector plate to create an aerosol. The droplet solvent progressively evaporates as the aerosol travels from the injection needle tip to the collector plate, and polymer nano- or microparticles are deposited on the grounded collector plate [26, 27]. The electrospraying technique has been shown successful to synthetize pure chitosan particles and chitosan loaded with dibasic calcium phosphate anhydrous (DCPA) by our group [25], and the addition of calcium phosphate to the chitosan provides a number of potential benefits such as being nucleus for extracellular matrix calcification and promoting cell adhesion and proliferation [27, 28]. Besides this initial synthesis of chitosan loaded with DCPA, more studies *are needed* to characterize the particles and *improve* the synthesis parameters.

Accordingly, the objectives of this study were to understand how electrospraying under different flow rates controls the properties of chitosan particles loaded with *DCPA* in terms of particle size, morphology, inorganic content, crystallinity, zeta potential, DCPA release, and minimum inhibitory concentration (MIC) against *S. mutans*.

Materials and Methods

Chitosan Purification

Commercial high-viscosity chitosan (Sigma Aldrich) was purified by dissolving 1 wt. % chitosan in a 3% acetic acid solution. The solution was then filtered and precipitated using 1M NaOH. The product was centrifuged at 5000 rpm for 5 min, the pellet was suspended in water, and NaOH was removed by dialysis. The purification process was repeated twice. *The chitosan used had degree of deacetylation of 98.5% and degrees of polymerization of 1890.*

Synthesis of Chitosan Particles Loaded with Calcium Phosphate

Chitosan (ChiP) and chitosan loaded with DCPA (DCPA/CHiP) particles were synthesized using the electrospray method. A solution was prepared with 10 mg/mL purified chitosan in 90 vol% acetic acid, and 2.5 mg/mL DCPA was added to this solution to synthesize chitosan particles loaded with DCPA. The solutions were electrosprayed at 30 kV, 18 cm from the solution injection needle to the collector. Three flow rates of 0.2, 0.5, or 1.0 mL/h were tested to optimize the synthesis conditions. The particles were deposited on a stainless-steel plate and crosslinked with glutaraldehyde vapor in a sealed container for 16 h.

Particle Characterization

Particle crosslinking was evaluated using two different methods: (1) Fourier transform infrared spectroscopy (FTIR) and (2) ninhydrin assay. Because the particle size and DCPA presence should not affect crosslinking, these tests were performed only for one group: DCPA/ChitP particles synthesized at a flow rate of 0.5 mL/h. FTIR was conducted using attenuated total reflectance (ATR) (Frontier, PerkinElmer, EUA), and spectra ranging from 4000 to 600 cm^{-1} were obtained with a resolution of 4 cm^{-1}. A ninhydrin assay was performed to detect free amino groups in the chitosan particles. Two milligrams of particles, with and without crosslinking treatment ($n = 3$), was dispersed in 0.5 mL of 2% ninhydrin solution and heated at 80 °C for 20 min. The samples were placed in an ice bath and centrifuged at 1200 rpm for 2 min. The absorbance of the solution was measured at 570 nm using a spectrophotometer (ELx800 Biotek, Winooski, USA). The percentage of primary amines was calculated by dividing the value of the crosslinked sample by that of the noncrosslinked sample.

Scanning electronic microscopy (SEM) was used to assess particle morphology and size (FEG 7401F, Jeol, Tokyo, Japan). Images were obtained at 20,000 × magnification, and at least 300 particles were measured using the ImageJ software (ImageJ, National Institutes of Health, Maryland, EUA).

The chitosan particles were analyzed using the DSC Q10 (TA instruments, New Castle, EUA) in the temperature range of 0 to 240 °C with a heating rate of 10 °C/min. The experiments were performed into the aluminum

pan under N_2 flow rate of 50 mL/min. The analysis used 1.17 mg of 1.0 mL/h DCPA/ChitP, 1.45 mg of 0.5 mL/h DCPA/ChitP, 1.79 mg of 0.2 mL/h DCPA/ChitP, and 1.39 mg of 0.5 mL/h ChitP. The first and second heating were recorded in order to obtain the thermal events with and without the thermal history of the particles, respectively.

In composites with organic and inorganic content, the amount of each one can be determined by thermogravimetric analysis (TGA) [29]. Therefore, in this study, the percentage of DCPA incorporated into the chitosan particles was determined by TGA (Model: sTAi 1500, Instrument Specialists Inc., Twin Lakes, WI, USA). The samples (4.5 mg) were heated from 30 to 950 °C at a rate of 10 °C/min under an air atmosphere, and ChitP at flow rate of 0.5 mL/h was used as control group.

DCPA/ChitP (*32 mg*) were immersed in deionized water at 37 °C, using a dialysis membrane; samples were collected at 1, 3, and 7 days after storage; and the calcium amount release from DCPA/ChitP was measured by inductive coupled plasma of optical emission spectroscopy (ICP-OES), after filtering the samples in a 22-µm filter.

Zeta potential was determined with particles dispersed in 10 mL of distilled water and sonicated using a 6 mm probe (Q500, Qsonica, Newtown, CT, USA) for 7 min in cycles of 1 s on and 3 s off and with a 20% amplitude. The solution was then subjected to light scattering analysis (Zetasizer Nano Zs, Malvern, Worcestershire, UK).

The minimum inhibitory concentration against *S. mutans* was determined using 12 serial concentrations of ChiP and DCPA/ChiP, from 50 to 0.02 mg/mL. Briefly, *S. mutans* was cultured in BHI (brain heart infusion (BHI) medium (Kasvi, São José dos Pinhais, Brazil) for 24 h at 37 °C in a 5% CO_2 atmosphere. Then, it was cultured in BHI agar plates (Kasvi), and individual colonies were dispersed in 0.9% NaCl to obtain solution absorbance of 0.135 at 660 nm (MR 96A, Mindray, São Paulo, SP, Brazil), which is equivalent to $1–2 \times 10^8$ UFC/mL [30]. A bacterial concentration of approximately $1–2 \times 10^5$ CFU/mL was obtained by adding 100 µL of the bacterial solution to 100 mL of BHI medium (Kasvi). The medium containing the microorganisms (200 µL/well) was added to a 96-well plate in addition to the synthetized ChiP or DCPA/ChiP particles. The samples were then incubated for 24 h at 37 °C in a 5% CO_2 atmosphere. A negative control group was tested in a culture medium with microorganisms without any particles, and a positive control group was tested in a culture medium without microorganisms or particles. After incubation, the absorbance at 570 nm was measured before the addition of 30 µL resazurin (Sigma Aldrich, São Paulo, Brazil) and after 2 h of incubation at 37 °C in a 5% CO_2 atmosphere. The minimum inhibitory concentration (MIC) was determined according to the absence of a statistical difference from the sample to the positive control group and a significant difference compared to the negative control group.

Statistical Analyses

Particle size data were analyzed using a two-way ANOVA and Tukey post-hoc test, with the flow rate and presence of DCPA as factors. One-way ANOVA was used to analyze the MIC of each group by comparing the absorbance of the samples to that of the control groups. All statistical tests were performed at a global significance level of 95% ($\alpha \leq 0.05$).

Results and Discussion

The present study showed that the electrospray technique used to produce ChiP and DCPA/ChiP particles with nano- to submicrometric sizes generated particles with differences in morphology, size distribution, zeta potential, MIC, and inorganic loading depending on the flow rate.

Chitosan is a natural polysaccharide that is stable at neutral pH but soluble in acidic solutions. In the present study, a glutaraldehyde crosslink of the particles was applied to decrease its solubility in acidic media and improve its applicability beyond sites of homeostasis with neutral pH, but also for inflammatory sites, which present a more acidic pH [31]. The FTIR spectra of DCPA/ChitP samples before and after crosslinking are shown in Fig. 1. After crosslinking (Fig. 1b), there was a reduction in the absorption band at 1557 cm^{-1}, corresponding to the N-H bending vibrations of the amino groups. The increase in the absorption band at 1655 cm^{-1} (N=C stretching) resulting from the crosslinking between chitosan and glutaraldehyde confirms the efficacy of the crosslinking process used for the particles, as previously described [32–34], and also it is efficient in providing crosslinking inside the particles without causing interparticle linkages, as observed in the SEM images in Fig. 2. In agreement, the results of the ninhydrin assay indicated that 48% of the amine groups were crosslinked with glutaraldehyde. The remaining 52% of free amine groups were responsible for the antimicrobial activity of the chitosan particles. The reaction of ninhydrin with amino acids resulted in a color change from yellow to light brown for crosslinked particles.

The morphologies of ChiP and DCPA/ChiP were similar under the three flow rate conditions, with only minor differences observed at the highest flow rate. The SEM images of ChiP (Fig. 2a–c) and DCPA/ChiP (Fig. 2d and e) particles synthesized at different flow rates showed irregular morphologies and a broad particle size distribution. The smaller particles presented a regular spherical shape, whereas the larger ones showed a central biconcave disc shape, with a height lower than the diameter on both sides. The particles

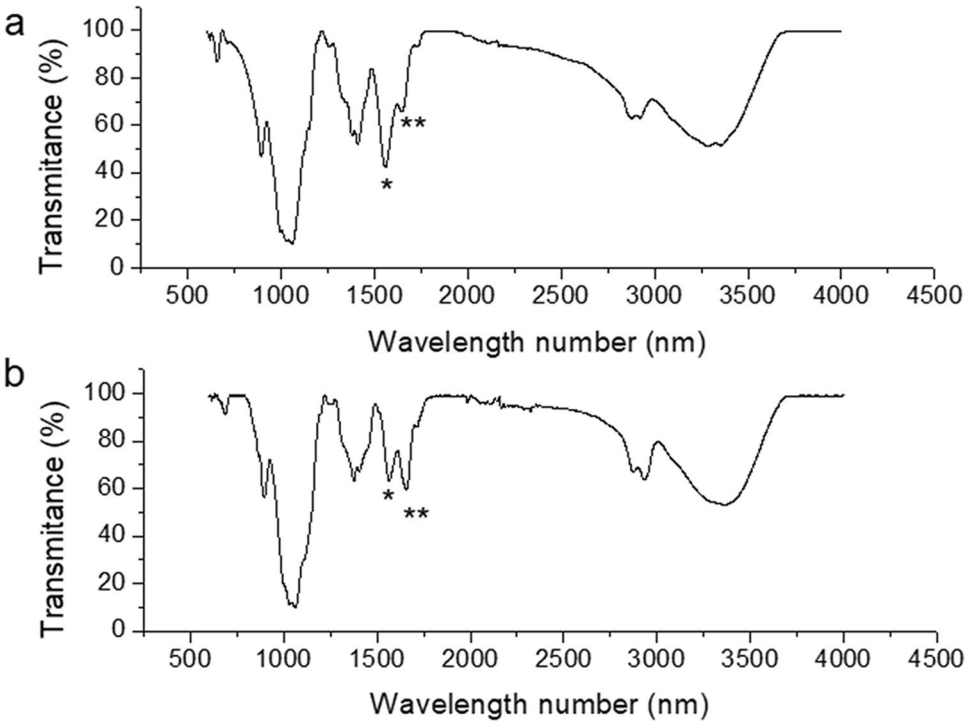

Fig. 1 FITR spectra of chitosan particles loaded with DCPA **a** before crosslinking with glutaraldehyde and **b** after crosslinking. *1557 cm^{-1} (N-H bending) and **1655 cm^{-1} (N=C stretching)

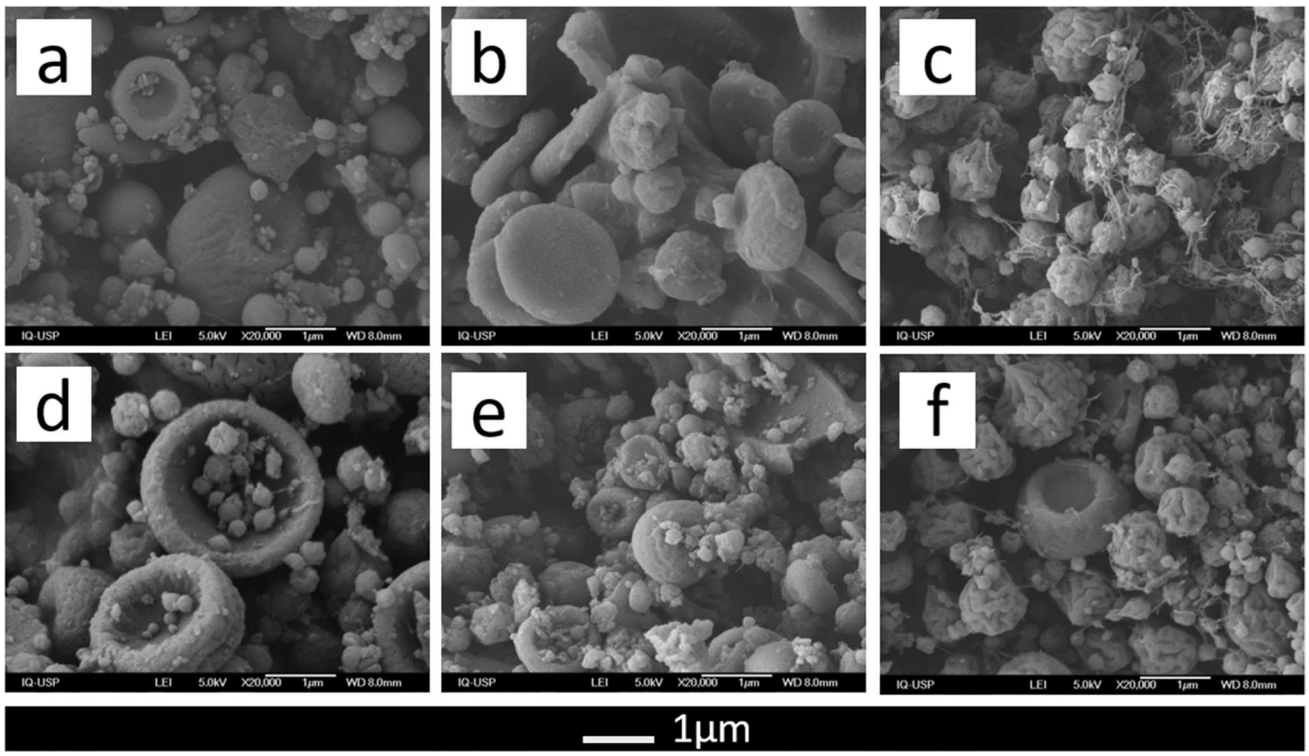

Fig. 2 Scanning electronic microscopy images taken at a magnification of 20,000× for chitosan particles synthetized with flow rate of **a** 0.2 mL/h, **b** 0.5 mL/h, **c** 1.0 mL/h and DCPA-loaded chitosan particles synthetized with flow rate of **d** 0.2 mL/h, **e** 0.5 mL/h, **f** 1.0 mL/h

synthesized at 1.0 mL/h (Fig. 2c and f), besides the smaller and greater particles described, also presented an intermediate particle size with a spherical shape and irregular surface forming grooves. In addition, fiber deposition between the particles was observed in this group. The addition of DCPA to the particles did not alter their morphology.

This finding was expected because the main parameters affecting particle morphology, such as solution concentration, viscosity, and conductivity [11, 35], were kept constant. The bi-concave disc shape observed for larger particles has been previously described [36, 37] and occurs because of the formation of a superficial polymeric pellicle, which shrinks as the solvents in the sprayed droplets evaporate. *Because the amount of solvent in particles with small and intermediary size is low, it was not enough to change the particle surface and form grooves as occurred in particles with larger size*. In the materials synthesized at the highest flow rate (1.0 mL/h), fibers were also observed among the particles. The electrospinning and electrospraying processes were similar, resulting in the deposition of fibers and particles, respectively. Changes in the synthesis parameters allow a crossing between the two processes, thus explaining the fibers found under the faster synthesis conditions [35].

Figure 3 shows the histograms of the particle size distributions. Statistical analysis indicated a similar mean size of particles obtained under the three flow rates for both chitosan particles (ChitP) and chitosan loaded with DCPA particles (DCPA/ChitP). Particle size analysis showed a broad distribution, ranging from 25 to 2500 nm, and they were similar to those reported in the literature for the electrospray of pure chitosan without crosslinking [27, 37, 38]. Depending on the clinical application, an appropriated distribution size of particles should be defined to avoid cytotoxicity. It was expected that the low flow rates would produce smaller-sized particles because smaller solution drops are formed in the needle and are easier to spray due to the electric field reducing the surface tension of the drop [11, 38]. In fact, despite the mean size of particles to be similar for all the experimental groups, the lower flow rate (0.2 mL/h) condition presented a higher percentage (29%) of particles in the nanometric scale (i.e., below 100 nm).

Differential scanning calorimetry (Fig. 4) does not show the glass transition (endothermic peak) for the particles prepared with 1.0 and 0.5 mL/h and 0.2 mL/h during the first and second heating. This amorphous structure agrees with the effect of the reticulation found for the glutaraldehyde

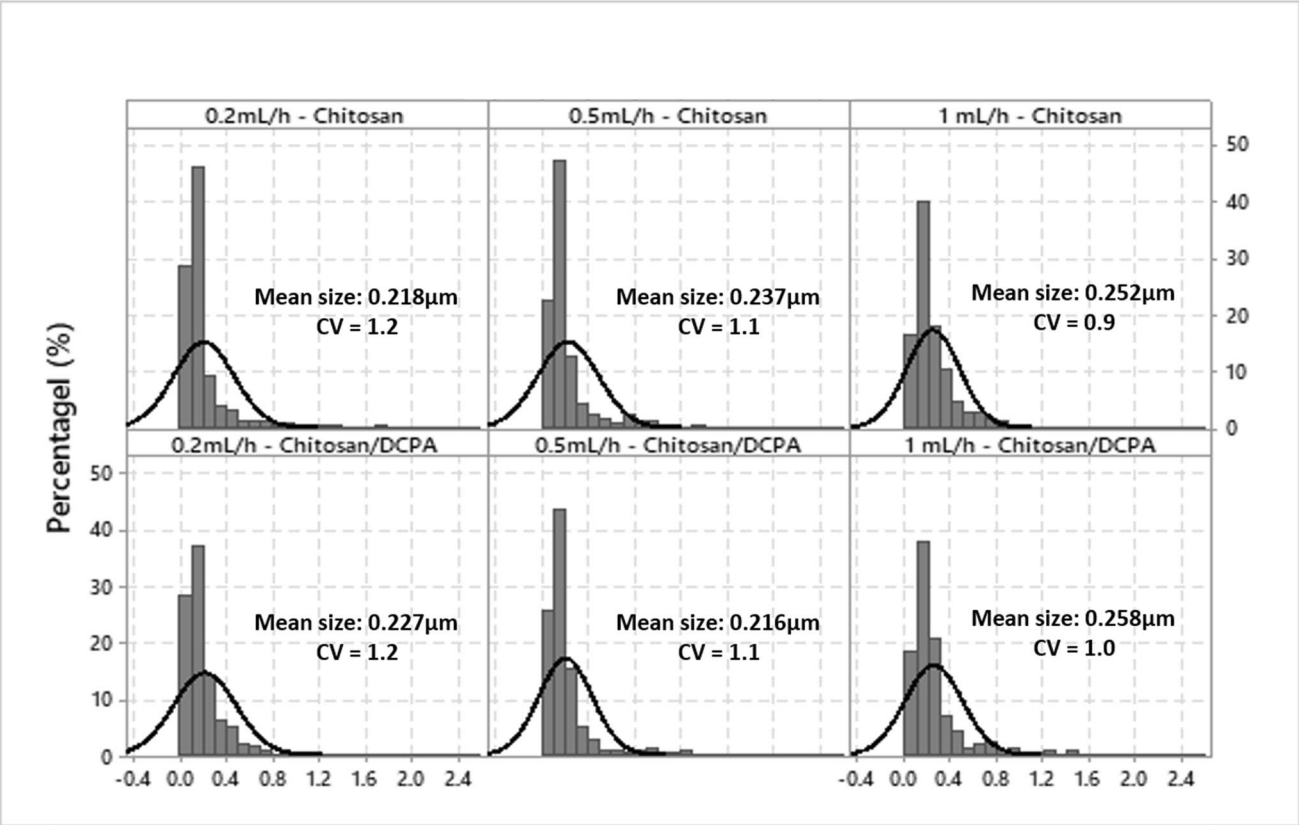

Fig. 3 Size distributions, *means size and coefficient of variation* of chitosan and DCPA/ChitP particles synthesized with flow rates of 0.2 mL/h, 0.5 mL/h, or 1 mL/h

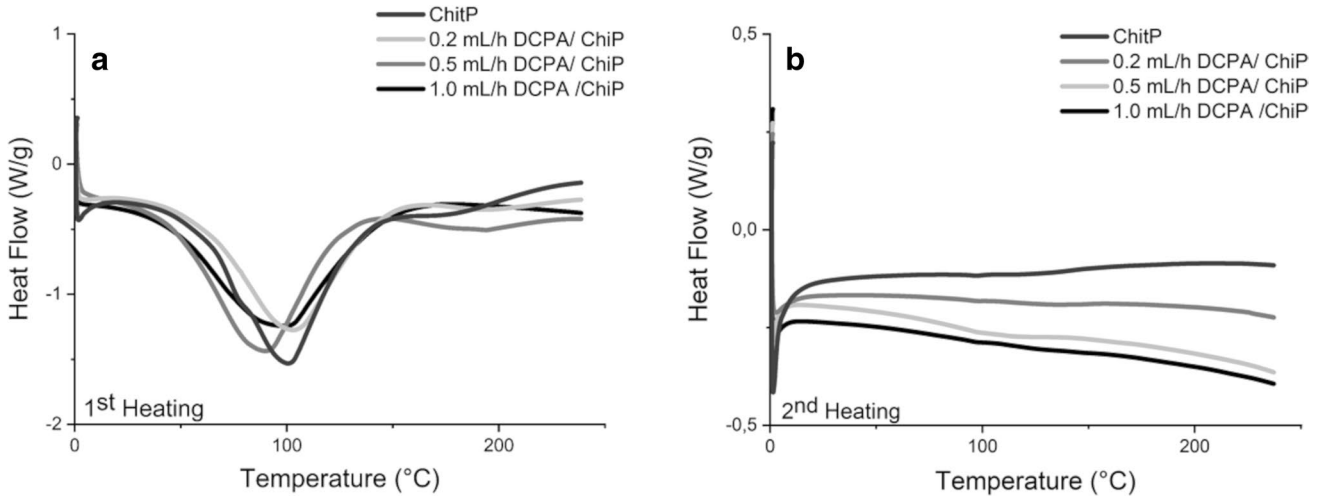

Fig. 4 DSC thermograms from the first heating (**a**) and the second heating (**b**) for the DCPA/ChitPa, with flow rates of 0.2 mL/h, 0.5 mL/h, or 1 mL/h and CHitP with 0.5mL/h flow rate

[39] and the tripolyphosphate (TPP) crosslinkers [40], and it also explains the water content showed by the endothermic peak from 50 to 100 °C (*evaporation*) [40, 41] during the first heating (Fig. 4b). This water absorption can trigger the DCPA release and also the particle disassembling.

The results of thermogravimetric analysis are shown in Fig. 5. It confirmed the incorporation of DCPA into chitosan particles. The materials synthesized at 0.5 mL/h and 1.0 mL/h presented similar results, with a residue of 10.4 and 9.9%, whereas only 5.9% was observed in the material synthesized at the lowest flow rate. These values are approximately 50% or 25% of the DCPA added to the initial solution. It is believed that during electrospray, the slow flow rate allows the DCPA to precipitate on the syringe, reducing its incorporation into the particles. The particles synthesized without DCPA showed no residue at flow rate of 0.5 mL/h.

Data from calcium released by DCPA/ChiP is presented on Fig. 6. There is no difference in the calcium amount *released from* the DCPA/ChitP in function of the time ($p = 0.627$) nor in function of the flow rate condition ($0 = 0.156$), being *released* on the average 12 mg calcium ions per gram of particles. This fast release *could be attributed* to the high solubility of DCPA [42] (Zhou), which was also observed in orthopedic cements [43]. The difference in the DCPA

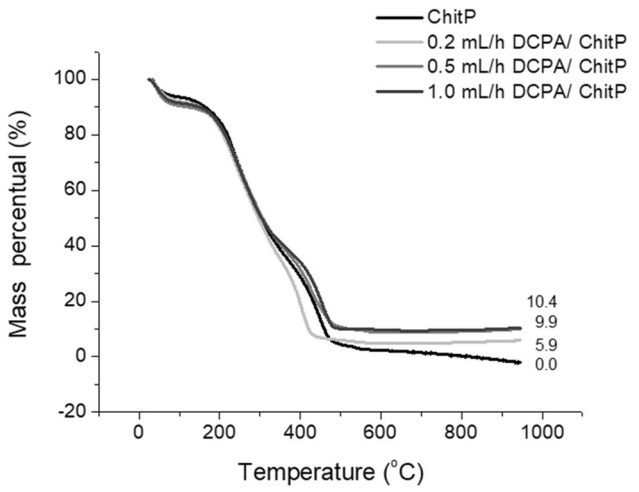

Fig. 5 Calcium ions released (mg) per gram of DCPA/ChitP with flow rates of 0.2 mL/h, 0.5 mL/h, or 1 mL/h after 24, 72, or 420 h in water

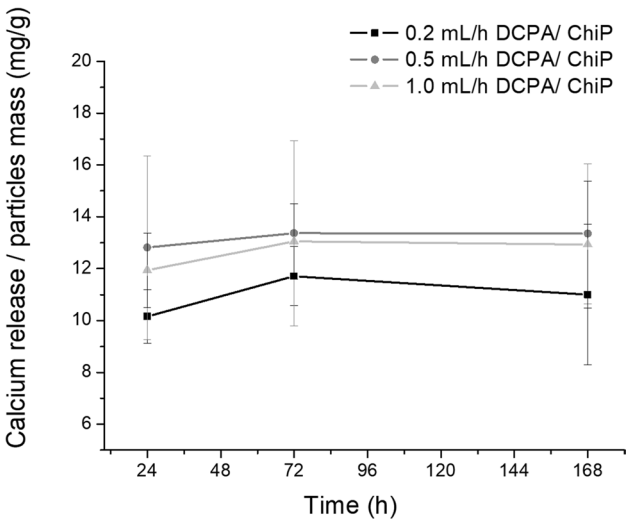

Fig. 6 Thermogravimetric analysis of chitosan (ChitP) and chitosan loaded with DCPA particles (DCPA/Chit) synthesized with flow rates of 0.2, 0.5, and 1.0 mL/h

incorporated during the synthesis was not enough to affect the calcium ion concentration released.

The zeta potential analysis is a way to estimate the degree of aggregation of the particles in the solution. When the zeta potential is closer to zero, the neutrality of the particles is higher as is the tendency for aggregation among them, allowing the formation of clusters. Values above 30 mV characterize strong cationic or anionic particles and indicate particle dispersion and stability in the solution [44, 45]. All tested conditions showed zeta potentials higher than 30 mV and ranged from 42 to 59 mV (Table I).

The positive charge observed in ChiP and DCPA/CHiP is derived from the free amine groups in the chitosan, which are protonated in aqueous solution. In the studied materials, the synthesis conditions had little effect on the zeta potential, which is most likely explained by the similar composition, morphology, and mean size of the particles [38, 46, 47]. The addition of DCPA to chitosan decreased the zeta potential, as phosphate ions have an affinity for protonated amine [48], resulting in a decrease in the positive charge of the particles.

Table I shows the minimum inhibitory concentrations (MIC) for different flow rates. The MIC of ChiP at a flow rate of 0.5 mL/h could not be estimated because it was over the maximum tested concentration (50 mg/mL) and DCPA/ChiP synthesized at 0.5 mL/h showed the lowest MIC (3.1 mg/mL). There was no relationship between the flow rate and MIC or particle size and MIC.

The MIC against *S. mutans* decreased by the addition of DCPA for the particles produced using the flow rate conditions of 0.2 and 0.5 mL/h, and it increased in the condition of 1.0 mL/h. In the last condition, this result can be explained by fewer protonated amine groups available to exert antimicrobial activity, as measured by the decrease in zeta potential [49–51]. On the other hand, the decrease in zeta potential for the lower flow rates was lower (approximately 11–12 mV) and appeared to be not strong enough by itself to increase the MIC, suggesting that other factors may have a leading role in determining the MIC. Each bacterial species has an optimum medium pH that favors their growth [52]. *S. mutans* is an acidogenic and acid-resistant bacterium with an optimum growth at pH 7.0 [53]. It is believed that the release of DCPA by DCPA/ChiP would increase the pH of the culture medium (initially set at 7.4), inhibiting *S. mutans* growth under conditions where the variation of zeta potential is lower. Comparing to particles of chitosan only, the condition with the highest antimicrobial inhibition (lower MIC) was the synthesis with 1.0 mL/h flow rate, followed by 0.2 and 0.5 mL/h conditions, respectively. This indicated a direct correlation with the zeta potential. In addition, the faster condition was the only condition in which nanofibers were observed. The nanofiber structure is expected to break during sample sonication, and the nano-sized fiber fragments would present a greater antimicrobial effect than the submicron particles [54].

Table I Zeta Potential and Minimum Inhibitory Concentration (MIC) of the Electrosprayed Chitosan Particles (ChitP) and Chitosan Loaded with DCPA (DCPA/ChiP) Particles Synthesized with Different Flow Rates

Flow rate	Material	Zeta potential (mV)	MIC (mg/mL)
0.2 mL/h	ChitP	58 ± 7	12.5
	DCPA/ChiP	47 ± 6	6.3
0.5 mL/h	ChitP	54 ± 8	-
	DCPA/ChiP	42 ± 5	3.1
1.0 mL/h	ChitP	59 ± 6	6.3
	DCPA/ChiP	43 ± 7	12.5

Conclusion

According to the observed results, it can be concluded that the chitosan particles loaded with DCPA that were synthesized at 0.5 mL/h gave the best overall properties. Particles synthesized using an intermediate flow rate presented lower MIC against *S. mutans* and high DCPA incorporation, in spite of *similar* calcium ions release. In addition, there was no fiber deposition at the intermediate flow rate, and the particles had a zeta potential well above 30 mV, precluding the formation of clusters.

Acknowledgements The authors thank the São Paulo Research Foundation, Brazil (FAPESP, 2016/13114-2), along with the FAPESP-UNSW Joint Research Grant Program, Brazil-Australia (FAPESP, 2017/50290-6) for funding this project.

Author contributions Lopes DP – chitosan purification, particles synthesis, TGA and drafting of the manuscript
Freitas SEM – MIC analysis, and drafting of the manuscript
Tanaka CB - conception, data interpretation and drafting of the manuscript
Delechiave G – zeta potential, DSC, and drafting of the manuscript
Kikuchi LNT – ninhydrin assay, FTIR and drafting of the manuscript
Braga RR - conception, data interpretation and reviewing of the manuscript
Kruzic JJ - conception, data interpretation and reviewing of the manuscript
Boaro LCC – MIC analysis, data interpretation and reviewing of the manuscript
Catalani LH - conception, data interpretation and reviewing of the manuscript
Moreira SM – ICO-OES, data interpretation and reviewing of the manuscript
Gonçalves F – MEV, statistical analysis conception, data interpretation and reviewing of the manuscript

Declarations

Conflict of Interest The authors declare no competing interests.

References

1. Demarco FF, Correa MB, Cenci MS, Moraes RR, Opdam NJ. Longevity of posterior composite restorations: not only a matter of materials. Dent Mater. 2012;28(1):87–101.
2. Mouhyi J, Dohan Ehrenfest DM, Albrektsson T. The peri-implantitis: implant surfaces, microstructure, and physicochemical aspects. Clin Implant Dent Relat Res. 2012;14(2):170–83.
3. Zandi H, Petronijevic N, Mdala I, Kristoffersen AK, Enersen M, Rocas IN, Siqueira-Jr J:F, Orstavik D. Outcome of endodontic retreatment using 2 root canal irrigants and influence of infection on healing as determined by a molecular method: a randomized clinical trial. J Endod. 2019;45(9):1089–98 e5.
4. Ahlfeld T, Doberenz F, Kilian D, Vater C, Korn P, Lauer G, Lode A, Gelinsky M. Bioprinting of mineralized constructs utilizing multichannel plotting of a self-setting calcium phosphate cement and a cell-laden bioink. Biofabrication. 2018;10(4):045002:1–33.
5. Anusavice KJ, Zhang NZ, Shen C. Controlled release of chlorhexidine from UDMA-TEGDMA resin. J Dent Res. 2006;85(10):950–4.
6. Rathke A, Staude R, Muche R, Haller B. Antibacterial activity of a triclosan-containing resin composite matrix against three common oral bacteria. J Mater Sci Mater Med. 2010;21(11):2971–7.
7. Khvostenko D, Hilton TJ, Ferracane JL, Mitchell JC, Kruzic JJ. Bioactive glass fillers reduce bacterial penetration into marginal gaps for composite restorations. Dent Mater. 2016;32(1):73–81.
8. Khvostenko D, Mitchell JC, Hilton TJ, Ferracane JL, Kruzic JJ. Mechanical performance of novel bioactive glass containing dental restorative composites. Dent Mater. 2013;29(11):1139–48.
9. Buruiana T, Melinte V, Popa ID, Buruiana EC. New urethane oligodimethacrylates with quaternary alkylammonium for formulating dental composites. J Mater Sci Mater Med. 2014;25(4):1183–94.
10. Imazato S, Ma S, Chen JH, Xu HH. Therapeutic polymers for dental adhesives: loading resins with bio-active components. Dent Mater. 2014;30(1):97–104.
11. Liang X, Soderling E, Liu F, He J, Lassila LV, Vallittu PK. Optimizing the concentration of quaternary ammonium dimethacrylate monomer in bis-GMA/TEGDMA dental resin system for antibacterial activity and mechanical properties. J Mater Sci Mater Med. 2014;25(5):1387–93.
12. Li F, Wang P, Weir MD, Fouad AF, Xu HH. Evaluation of antibacterial and remineralizing nanocomposite and adhesive in rat tooth cavity model. Acta Biomater. 2014;10(6):2804–13.
13. Kim J-S, Shin D-H. Inhibitory effect on Streptococcus mutans and mechanical properties of the chitosan containing composite resin. Restor Dent Endod. 2013;38(1):36–42.
14. Costa EM, Silva S, Veiga M, Tavaria FK, Pintado MM. A review of chitosan's effect on oral biofilms: perspectives from the tube to the mouth. J Oral Biosci. 2017;59(4):205–10.
15. Petri DF, Donega J, Benassi AM, Bocangel JA. Preliminary study on chitosan modified glass ionomer restoratives. Dent Mater. 2007;23(8):1004–10.
16. Di Martino A, Sittinger M, Risbud MV. Chitosan: a versatile biopolymer for orthopaedic tissue-engineering. Biomaterials. 2005;26(30):5983–90.
17. Yan N, Chen X. Don't waste seafood waste. Nature. 2015;524(7564):155–7.
18. Skrtic D, Antonucci JM, Eanes ED. Improved properties of amorphous calcium phosphate fillers in remineralizing resin composites. Dent Mater. 1996;12(5):295–301.
19. Chiari MD, Rodrigues MC, Xavier TA, de Souza EM, Arana-Chavez VE, Braga RR. Mechanical properties and ion release from bioactive restorative composites containing glass fillers and calcium phosphate nano-structured particles. Dent Mater. 2015;31(6):726–33.
20. Xu HH, Moreau JL. Dental glass-reinforced composite for caries inhibition: calcium phosphate ion release and mechanical properties. J Biomed Mater Res B Appl Biomater. 2010;92(2):332–40.
21. Jayasuriya AC, Bhat A. Optimization of scaled-up chitosan microparticles for bone regeneration. Biomed Mater. 2009;4(5):e055006.1-8.
22. Jayasuriya AC, Bhat A. Fabrication and characterization of novel hybrid organic/inorganic microparticles to apply in bone regeneration. J Biomed Mater Res A. 2010;93(4):1280–8.
23. Yunoki A, Tsuchiya E, Fukui Y, Fujii A, Maruyama T. Preparation of inorganic/organic polymer hybrid microcapsules with high encapsulation efficiency by an electrospray technique. ACS Appl Mater Interfaces. 2014;6(15):11973–9.
24. Randolph LD, Palin WM, Leloup G, Leprince JG. Filler characteristics of modern dental resin composites and their influence on physico-mechanical properties. Dent Mater. 2016;32(12):1586–99.
25. Tanaka CB, Lopes DP, Kikuchi LNT, Moreira MS, Catalani LH, Braga RR, Kruzic JJ, Gonçalves F. Development of novel dental restorative composites with dibasic calcium phosphate loaded chitosan fillers. Dent Mater. 2020;36(4):551–9.
26. Sridhar R, Ramakrishna S. Electrosprayed nanoparticles for drug delivery and pharmaceutical applications. Biomatter. 2013;3(3).
27. Thien DVH, Hsiao SW, Ho MH. Synthesis of electrosprayed chitosan nanoparticles for drug sustained release. Nano LIFE. 2012;2(1):1–11.
28. Lim SS, Chai CY, Loh HS. In vitro evaluation of osteoblast adhesion, proliferation and differentiation on chitosan-TiO. Mater Sci Eng C Mater Biol Appl. 2017;76:144–52.
29. Aydınoğlu A, Yoruç ABH. Effects of silane-modified fillers on properties of dental composite resin. Mater Sci Eng C Mater Biol Appl. 2017;79:382–9.
30. CLSI. Clinical and laboratory standards institute standards development policies and process 2013.
31. Hazehara-Kunitomo Y, Hara ES, Ono M, Aung KT, Komi K, Pham HT, Akiyama K, Okada M, Oohashi T, Matsumoto T, Kuboki T. Acidic pre-conditioning enhances the stem cell phenotype of human bone marrow stem/progenitor cells. Int J Mol Sci. 2019;20(5):e1097. 1-10.
32. Gonsalves AA, Araújo CRM, Soares NA, Goulart MOF, Abreu FC. Diferentes estratégias para a reticulação de quitosana. Quim Nova. 2011;34(7):1215–23.
33. Mendes AA, Oliveria PC, Castro HF, Giordano RLC. Aplicação de quitosana como suporte para a imobilização de enzimas de interesse industrial. Quim Nova. 2011;34(5):831–40.
34. Odaci D, Timur S, Telefoncu A. A microbial biosensor based on bacterial cells immobilized on chitosan matrix. Bioelectrochemistry. 2009;75(1):77–82.
35. Gomez-Mascaraque LG, Sanchez G, Lopez-Rubio A. Impact of molecular weight on the formation of electrosprayed chitosan microcapsules as delivery vehicles for bioactive compounds. Carbohydr Polym. 2016;150:121–30.
36. Kawakami K, Sumitani C, Yoshihashi Y, Yonemochi E, Terada K. Investigation of the dynamic process during spray-drying to improve aerodynamic performance of inhalation particles. Int J Pharm. 2010;390(2):250–9.
37. Zhang S, Kawakami K. One-step preparation of chitosan solid nanoparticles by electrospray deposition. Int J Pharm. 2010;397(1-2):211–7.
38. Songsurang K, Praphairaksit N, Siraleartmukul K, Muangsin N. Electrospray fabrication of doxorubicin-chitosan-tripolyphosphate nanoparticles for delivery of doxorubicin. Arch Pharm Res. 2011;34(4):583–92.

39. Klein, M. P.; Nunes, M. R.; Rodrigues, R. C.; Benvenutti, E. V; Costa, T. M. H.; Hertz, P. F.; Ninow, J. L. Effect of the support size on the properties of β-galactosidase immobilized on chitosan: advantages and disadvantages of macro and nanoparticles. Biomacromolecules 2012; 13(8):2456–2464. https://doi.org/10.1021/bm3006984.
40. Michailidou G, Ainali NM, Xanthopoulou E, Nanaki S, Kostoglou M, Koukaras EN, Bikiaris DN. Effect of poly(vinyl alcohol) on nanoencapsulation of budesonide in chitosan nanoparticles via ionic gelation and its improved bioavailability. Polymers (Basel). 2020;12(5):1101. https://doi.org/10.3390/polym12051101.
41. Shetta A, Kegere J, Mamdouh W. Comparative study of encapsulated peppermint and green tea essential oils in chitosan nanoparticles: encapsulation, thermal stability, in-vitro release, antioxidant and antibacterial activities. Int. J. Biol. Macromol. 2019;126:731–42. https://doi.org/10.1016/j.ijbiomac.2018.12.161.
42. Zhou H, Yang L, Gbureck U, Bhaduri SB, Sikder P. Monetite, An important calcium phosphate compound–Its synthesis, properties and applications in orthopedics. Acta Biomater. 2021;127:41–55. https://doi.org/10.1016/j.actbio.2021.03.050.
43. Wang X, Ye J, Wang Y. Hydration mechanism of a novel PCCP + DCPA cement system. J Mater Sci Mater Med. 2007;19(2):813–6. https://doi.org/10.1007/s10856-006-0029-6.
44. Clogston JD, Patri AK. Zeta potential measurement. Methods Mol Biol. 2011;697:63–70.
45. Salopek B, Krasic D, Filipovic S. Measurement and application of zeta-potential. Rudarsko-geoloiko-naftni zbornik. 1992;4:147–51.
46. Alqahtani FY, Aleanizy FS, Tahir EE, Alquadeib BT, Alsarra IA, Alanazi JS, Abdelhady HG. Preparation, characterization, and antibacterial activity of diclofenac-loaded chitosan nanoparticles. Saudi Pharm J. 2019;27(1):82–7.
47. Wiarachai O, Thongchul N, Kiatkamjornwong S, Hoven VP. Surface-quaternized chitosan particles as an alternative and effective organic antibacterial material. Colloids Surf B Biointerfaces. 2012;92:121–9.
48. Stefano C, Gianguzza A, Piazzese D, Sl S. Speciation of chitosan–phosphate and chitosan–nucleotide systems in NaCI aqueoussolution. Chemical Speciation & Bioavailability. 2015;22(2):99–107.
49. Goy RC, Britto D, Assis OBG. Review of the antimicrobial activity of chitosan. Polímeros: Ciência e Tecnologia. 2009;19(3):241–7.
50. Kong M, Chen XG, Xing K, Park HJ. Antimicrobial properties of chitosan and mode of action: a state of the art review. Int J Food Microbiol. 2010;144(1):51–63.
51. Perinelli DR, Fagioli L, Campana R, Lam JKW, Baffone W, Palmieri GF, Casettari L, Bonacucina G. Chitosan-based nanosystems and their exploited antimicrobial activity. Eur J Pharm Sci. 2018;117:8–20.
52. Davey KR. Modelling the combined effect of temperature and pH on the rate coefficient for bacterial growth. Int J Food Microbiol. 1994;23(3-4):295–303.
53. Castillo A, Rubiano S, Gutiérrez J, Hermoso A, Liébana J. Post-pH effect in oral streptococci. Clin Microbiol Infect. 2000;6(3):142–6.
54. Sarwar A, Katas H, Zin NM. Antibacterial effects of chitosan–tripolyphosphate nanoparticles: impact of particle size molecular weight. J Nanopart Res. 2014; 16:e2517.1-14.